The Journal of Eukaryotic Microbiology

ISOP Published by the International Society of Protistologists

Journal of Eukaryotic Microbiology ISSN 1066-5234

ORIGINAL ARTICLE

Studies on Woloszynskioid Dinoflagellates X: Ultrastructure, Phylogeny and Colour Variation in *Tovellia rubescens* n. sp. (Dinophyceae)

Mariana S. Pandeirada[a,b], Sandra C. Craveiro[a,b], Niels Daugbjerg[c], Øjvind Moestrup[c], Pedro Domingues[d] & António J. Calado[a,b]

a Department of Biology, University of Aveiro, Aveiro, P-3810-193, Portugal
b GeoBioTec Research Unit, University of Aveiro, Aveiro, P-3810-193, Portugal
c Marine Biological Section, Department of Biology, University of Copenhagen, Universitetsparken 4, Copenhagen Ø, DK-2100, Denmark
d Mass Spectrometry Centre, Department of Chemistry & QOPNA, University of Aveiro, Aveiro, P-3810-193, Portugal

Keywords
Astaxanthin; central pyrenoid complex; flagellar apparatus; ITS1-5.8S-ITS2 rDNA; LSU rDNA; Tovelliaceae.

Correspondence
A.J. Calado, Department of Biology, University of Aveiro, P-3810-193 Aveiro, Portugal
Telephone number: +351 234370785; FAX number: +351 234372587; e-mail: acalado@ua.pt

Received: 23 March 2019; revised 2 May 2019; accepted June 4, 2019.
Early View publication June 30, 2019

doi:10.1111/jeu.12745

ABSTRACT

The external morphology and internal cell fine structure of a new species of Tovelliaceae, *Tovellia rubescens* n. sp., is described. Phylogenetic analyses based on partial LSU rDNA sequences place the new species in a clade containing *Tovellia* species that accumulate red pigments and identify *T. aveirensis* as its closest known relative. Cells of *T. rubescens* n. sp. were mostly round and had the cingulum located near the middle, with its ends displaced about one cingular width. Small numbers of distinctly flat cells appeared in culture batches; their significance could not be determined. Cells of the new species in culture batches progressively changed from a yellowish-green, mainly due to chloroplast colour, to a reddish-brown colour that appeared associated with lipid bodies. The switch to a reddish colour happened earlier in batches grown in medium lacking sources of N or P. Pigment analyses by HPLC-MS/MS revealed the presence of astaxanthin and astaxanthin-related metabolites in the new species, but also in *T. aveirensis*, in which a reddish colour was never observed. The chloroplast arrangement of *T. rubescens* n. sp. resembled that of *T. aveirensis*, with lobes radiating from a central pyrenoid complex. The flagellar apparatus and pusular system fell within the general features described from other Tovelliaceae. A row of microtubules interpretable as a microtubular strand of the peduncle was present. Spiny resting cysts with red contents and an ITS sequence identical to that of cultured material of the new species were found in the original locality.

THE dinoflagellates commonly designated "woloszynskioids" are artificially linked by the presence of an amphiesma with fewer vesicles than typical gymnodinioids, but with amphiesmal vesicles more numerous and containing thinner plate-like material than typical peridinioid or gonyaulacoid species (Lindberg et al. 2005). The name of this artificial assemblage stems from the generic name *Woloszynskia* R.H. Thompson, originally proposed to accommodate species previously classified as *Gymnodinium* F. Stein in which a thin theca had been demonstrated (Thompson 1951, p. 286). The genus was found to be polyphyletic, as initially suggested by Stosch (1973), who pointed out the presence of different cyst and eyespot types within the group of species assigned to *Woloszynskia* (Lindberg et al. 2005). Most species of woloszynskioids are currently recognized as members of different dinoflagellate groups, which are partly characterized by one or a few distinct eyespot types. Species with an eyespot made of more or less fused, carotenoid-rich oil globules not surrounded by membranes are currently grouped in their own family and order, respectively named Tovelliaceae and Tovelliales (Moestrup and Calado 2018). Species of Tovelliaceae studied ultrastructurally have been shown to share several distinctive features of their

flagellar and pusular apparatuses (Calado 2011) and provide useful comparison points.

The genus *Tovellia* Moestrup, K. Lindberg and Daugbjerg currently includes about a dozen species that bear peridinin-containing, yellowish-green or brownish-green chloroplasts (Pandeirada et al. 2017; Zhang et al. 2016). However, in a group of species that appear to be phylogenetically related the cells often show a distinct reddish colour, and blooms of these species may result in a spectacular blood-red colouration of the water (Moestrup et al. 2006; Zhang et al. 2016). In two of these species, *T. sanguinea* Moestrup, Gert Hansen, Daugbjerg, Flaim and d'Andrea and *T. diexiensis* Qi Zhang and G. X. Liu, the red carotenoid astaxanthin was shown to be abundant in the cells (Frassanito et al. 2006; Zhang et al. 2016). A new species of *Tovellia* with cell colour varying from yellowish-green to reddish-brown is described herein on the basis of light, scanning electron and transmission electron microscopy, and placed by partial LSU rDNA-based phylogenetic analysis within the clade that includes the red-coloured species. Pigment analysis by HPLC-MS revealed the presence of astaxanthin and related metabolites. The new species is the third species of *Tovellia* to be reported from continental Portugal (Pandeirada et al. 2013, 2014, 2017).

MATERIALS AND METHODS

Biological material

The species described herein was found in the plankton of a shallow, freshwater pond in Gafanha da Boavista, Ílhavo, Portugal (40°35′44.70″N, 8°41′49.66″W), sampled on 28 October 2010. A culture was started from the isolation of a single cell from this sample into quadruple concentration L16 medium (Lindström 1991) supplemented with vitamins according to Popovský and Pfiester (1990) — 4 × L16 + vit. A second isolate from the same pond, collected on 18 August 2011, proved identical in morphology and LSU rDNA sequence and was also used for observations and experiments. Maintenance of cultures and all experiments were conducted in a chamber at 18 °C with 12 h:12 h light:dark photoperiod and photon flux density about 25 μmol/m^2/s. Resting cysts were isolated from the same pond into the same conditions, but failed to produce viable cultures; the cysts were similar to one another in morphology and the ITS1-5.8S-ITS2 rDNA sequence established from one of them was 100% identical to that obtained from the culture started in October 2010. Attempts to induce sexual reproduction included isolation of about 20 cells into 250 μl of either full medium, or the same medium with sources of nitrogen excluded, or the same medium without phosphate; alternatively, about 20 cells of each culture line were mixed into 250 μl of full or either nitrogen- or phosphate-deficient medium. These experiments were conducted in 96-well cell culture plates (Sarstedt, Numbrecht, Germany). For the experimental induction of production of astaxanthin-related compounds, see below.

Light microscopy (LM)

Light micrographs of swimming cells, dividing cells and resting stages were taken with a Zeiss Axioplan 2 imaging light microscope (Carl Zeiss, Oberkochen, Germany), using DP70 and ColorView IIIu Olympus cameras (Olympus Corp., Tokyo, Japan). Cells emerging from division cysts were recorded with a JVC TK-C1481BEG colour video camera (Norbain SD Ltd, Reading, U.K.), coupled to a Leitz Labovert FS inverted light microscope (Leica Microsystems, Wetzlar, Germany).

Scanning electron microscopy (SEM)

Swimming cells were fixed by mixing equal portions of cell suspension and a fixative containing a 1:5 proportion of saturated $HgCl_2$ solution and 2% OsO_4 for 15 min, and further processed as detailed in Daugbjerg et al. (2014) for the Portuguese material of *Borghiella andersenii* Daugbjerg, Andreasen, Happel, Pandeirada, Gert Hansen, Craveiro, Calado and Moestrup. The material was critical point dried in a Baltec CPD-030 (Balzers, Liechtenstein), mounted on stubs, sputter coated with gold palladium and observed in a Hitachi S-4100 scanning electron microscope (Hitachi High-Technologies Corp., Tokyo, Japan).

Transmission electron microscopy (TEM)

Vegetative cells with reddish-brown colour were prepared for TEM as in Pandeirada et al. (2014). Serial sections of one cell were observed with a JEM 1010 electron microscope (JEOL Ltd., Tokyo, Japan) and images recorded with a Gatan Orius digital camera (Gatan, Inc., Pleasanton, CA).

HPLC-MS and HPLC-MS/MS characterization of pigment extract

The pigment composition of cultures of the new species grown in full and N-deficient medium was compared to that of cultures of *Tovellia aveirensis* Pandeirada, Craveiro, Daugbjerg, Moestrup and Calado grown in similar conditions. For the sake of clarity, the new species, which is formally described at the end of the text, is hereafter referred by its proposed name, *T. rubescens* n. sp. Pigments were separated on a HPLC system (Waters Alliance 2690, Milford, MA) coupled to a linear ion trap mass spectrometer LXQ (ThermoFinnigan, San Jose, CA). Cultures of *T. rubescens* n. sp. and *T. aveirensis* were grown for about 20 d in 50-ml tissue culture flasks (Sarstedt) with 4 × L16 + vit or the equivalent N-deficient medium. To compensate for the reduced growth supported by the N-deficient medium, the contents of two flasks were pooled, thereby increasing cell numbers for pigment extraction. The number of cells filtered for pigment extraction was, for *T. aveirensis*, about 68,900 cells grown in N-deficient medium, and some 133,800 in the full medium. For *T. rubescens* n. sp., about 108,000 cells were collected from each growth condition. The cells were harvested

with nylon filters (Pall membrane filters, Nylaflo membrane, diam. 25 mm, pore size 0.45 μm) and the pigments were extracted through the following steps: (i) 2 ml of acetone for about 3 min, followed by 2 ml of methanol; (ii) another 2 ml of acetone immediately followed by 2 ml of methanol. The extract was then dried under a controlled stream of nitrogen, and dissolved in 100 μl of 50% methanol in water. A volume of 5 μl of this solution was introduced into a Supelco Bio Wide Pore C5 column (15 cm × 0.5 mm, 5 μm; Supelco, Bellefonte, PA). The mobile phase A consisted of 95% water and 5% acetonitrile with 0.1% of formic acid. The mobile phase B consisted of 100% methanol. The mobile phase gradient was programmed as follows: the initial conditions were 50% of B for 2 min; 2–42 min linear gradient to 100% of B; 42–50 min isocratic at 100% of B, and the flow rate was 10 μl/min, obtained using a house-made splitter. To obtain the product-ion spectra of the major components during LC experiments, cycles consisting of one full scan mass spectrum in the *m/z* range from 70 to 1,000, and three data-dependent MS/MS scans were repeated continuously throughout the experiments with the following dynamic exclusion settings: repeat count 3; repeat duration 15 s; exclusion duration 45 s. The LXQ was operated in positive mode (electrospray voltage + 5 kV), with a capillary temperature of 275 °C and a sheath gas flow of 8 AU (arbitrary units). Normalized collision energy™ (CE) was set to 35 AU for MS/MS experiments. Data acquisition was carried out on an Xcalibur data system (V2.0).

Single-cell polymerase chain reaction (PCR)

Cells of both culture lines were used for PCR amplification of ca. 1,500 base pairs (bp) of the LSU rDNA. Cells of the culture line started in October 2010 and resting cysts from field samples were used for amplification of ca. 600 bp of ITS1-5.8S-ITS2 rDNA. In all cases, single swimming cells or single cysts were transferred to 0.2-ml PCR tubes and immediately frozen at −8 °C for 4 d, before PCR reactions. LSU rDNA amplification involved the use of the terminal primers D1R (Scholin et al. 1994) and 28-1483R (Daugbjerg et al. 2000). PCR amplifications were based on the illustra™ puReTaq Ready-To-Go PCR Beads kit (GE Healthcare, UK Ltd., Buckinghamshire, U.K.), and used the thermocycler Biometra-Tprofessional (Biometra GmbH, Göttingen, Germany). The thermal profile was as outlined in Pandeirada et al. (2014). The same thermocycler was used for ITS amplifications, which were carried out according to Takano and Horiguchi (2005), with one modification: the external primer LSU R2 used in the first round of amplification was replaced by the primer 28-1483R mentioned above. PCR products from all amplifications were loaded on a 1% agarose gel, run for 20 min at 90 V and viewed on a UV light table (Molecular imager chemi-Doc XRS System, Bio-Rad Laboratories, Inc., Hercules, CA). To increase the amount of LSU rDNA products, a nested-PCR was performed using 1 μl from the first PCR products in two PCR reactions with two combinations of primers: D1R-D3B and D3A-28-1483. The thermal profile can be found in Pandeirada et al. (2017). The PCR products were purified using the QIAquick PCR Purification Kit (Qiagen), following the manufacturer's recommendations, and sent to Macrogen Europe (Amsterdam, The Netherlands) for sequence determination. The sequencing primers for LSU rDNA were the same as in Pandeirada et al. (2014), while those for ITS were those listed in Takano and Horiguchi (2005).

Alignment and phylogenetic analyses

Two alignments (alignment 1 and 2) were performed for this study. In alignment 1 the LSU rDNA sequence of *Tovellia rubescens* n. sp. was added to the alignment recently used to infer the phylogeny of the congener *T. rinoi* Pandeirada, Craveiro, Daugbjerg, Moestrup and Calado (see details in Pandeirada et al. 2017). Alignment 1 included 1,151 base pairs (domain D2 was deleted due to possible alignment ambiguities when including a systematic broad range of dinoflagellates and outgroup taxa). To examine the phylogenetic position of the recently described *T. diexiensis*, a red *Tovellia* species that could not be included in alignment 1 because the known part of its LSU rDNA sequence was too short, a second alignment was prepared. In alignment 2 only dinoflagellates in the Tovelliaceae were included. This allowed inclusion of domain D2, and the alignment included 714 base pairs (from 27 upstream domain D1 to 7 base pairs downstream domain D2 following the secondary structure model by Lenaers et al. 1989). Both alignment 1 and 2 were used to infer the phylogeny using Bayesian (MrBayes, ver. 3.2.2 x64, Ronquist and Huelsenbeck 2003) and maximum likelihood analyses (PhyML, ver. 3.0, Guindon and Gascuel 2003). Bayesian analyses were run on a local computer with 5 million generations, and trees were sampled every 1,000th generation. The burn-in was evaluated by plotting the LnL values as a function of generations. Burn-in occurred after 501.000 generations (conservative number) resulting in the removal of 501 trees in both Bayesian analyses (alignment 1 and 2). This left 4,500 trees as input for 50% majority-rule consensus trees in PAUP* (Swofford 2003). jModelTest (ver. 2.1.7, Darriba et al. 2012) was used to find the best fit model for the data matrices and the model chosen was GTR + I + G (i.e. general time-reversible with the proportion of invariable sites and gamma distribution). The Montpellier bioinformatics platform at http://www.atgc-montpellier.fr/phyml was used to run PhyML analyses, and the robustness of clades was evaluated with 1,000 bootstrap replications. Values (≥ 50%) were plotted on Bayesian trees when identical topologies were suggested.

Outgroup taxa

In alignment 1 the diverse assemblage of dinoflagellates (78 taxa) was rooted with three ciliates, four apicomplexan and one perkinsozoan species. Based on the tree topology from aligment 1 *Jadwigia applanata* Moestrup, K. Lindberg

and Daugbjerg was used to root *Bernardinium bernardinense* Chodat and *Tovellia* spp. in alignment 2.

RESULTS

General morphology (LM and SEM)

Vegetative cells of *T. rubescens* n. sp. are illustrated by LM and SEM in Fig. 1A–2H and 3A–E, respectively. Epi- and hypocone were similar in size, the epicone nearly hemispherical and the hypocone hemispherical to rounded conical, sometimes with a pointed antapex (Fig. 1A–2D, 3A–C). The epicone was usually slightly projected near the apex, at the level of the apical line of plates (ALP, see below) (Fig. 1B, E). The cingulum was displaced about one cingulum width (Fig. 1A–D, 2A–D, 3A–C). Cells were slightly compressed dorsoventrally, with the hypocone somewhat obliquely flattened in lateral view (Fig. 1F). Cells were 18.5–43 μm long, 12.5–33 μm wide (n = 54 for both measurements) and 11.5–28 μm thick (n = 37). Chloroplasts were yellowish-green with lobes radiating from the centre (Fig. 1B, D, E). A large, bright-red eyespot was located across the anterior to middle part of the sulcus; its length was mostly 4–8 μm, and it appeared independent of chloroplast lobes (Fig. 1A, C, E, F). The nucleus was usually transversely elongated along the dorsal side of the hypocone (Fig. 1B, F, 2E); in a few smaller cells, it was ellipsoid and extended to the middle of the cell (Fig. 2D). The amphiesma lining swimming cells was usually undetectable, but revealed the presence of thin amphiesmal plates when shed (Fig. 2E).

Colour variation of vegetative cells

Yellowish-green cells of *T. rubescens* n. sp. usually displayed two types of cytoplasmic inclusions: brownish-yellow accumulation bodies in the epicone (Fig. 1F), and reddish granules with an eyespot-like colour in the hypocone (Fig. 1B, D, E). Old, dense cultures grown in full medium, and ca. 10-d old batches grown in medium without nitrogen or phosphorus, often showed darker cells with a more distinctly reddish-brown colour. These cells accumulated red to brown granules, usually first in the hypocone (Fig. 1E, 2A, B), but eventually over the entire cell, masking the colour of chloroplasts (Fig. 2C–H). Reddish-brown cells were usually of similar shape to the yellowish-green cells of less dense batches (Fig. 2C–E). However, morphologically distinct cells were regularly found in low numbers in red-coloured batches; these cells were nearly circular in ventral view, were strongly flattened dorsoventrally, and often had a wavy or denticulate outline, especially on the hypocone (Fig. 2F–H).

Structure of the amphiesma (SEM)

The epi- and hypocone were covered by numerous pentagonal or hexagonal plates arranged in roughly six latitudinal series on the epicone and four or five on the hypocone (Fig. 3A–C, E). The cingulum was lined by two series of amphiesmal vesicles, the anterior one with rectangular or pentagonal plates abutting the sharply defined anterior edge, and the posterior one with roughly hexagonal plates that extended onto the hypocone, over the rounded posterior cingulum edge (Fig. 3A–C). A line of narrow amphiesmal vesicles (apical line of plates—ALP) extended from the ventral side, nearly above the sulcus, over the apex, and ended on the dorsal side; one plate usually separated the ventral end of the ALP from the proximal end of the cingulum, and there were two (seldom three) plates between ALP and cingulum on the dorsal side (Fig. 3A–D). The ALP amphiesmal vesicles were 0.2–0.4 μm wide (n = 22), and usually displayed one or several axial knobs (Fig. 3D). The length of ALP vesicles was difficult to

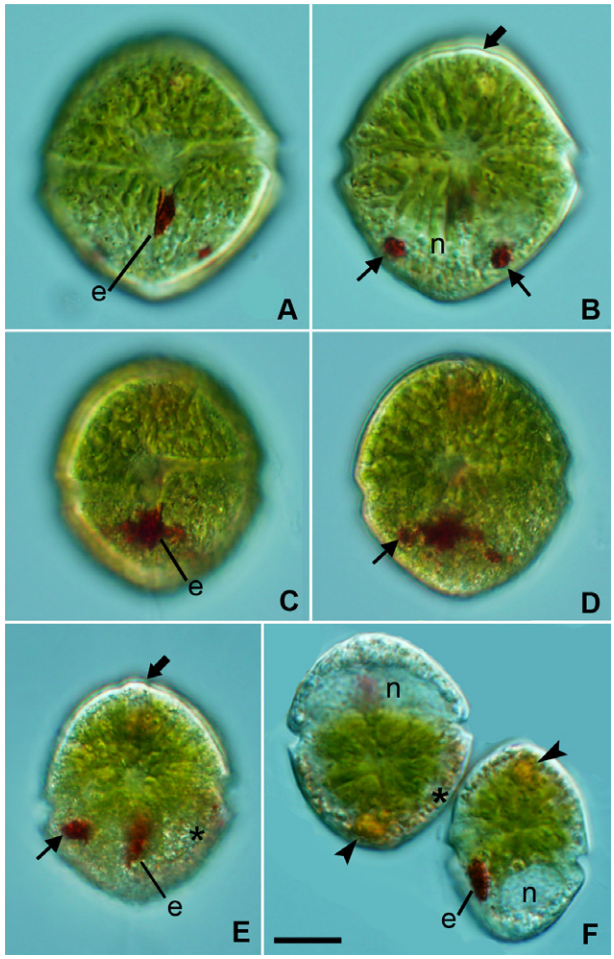

Figure 1 *Tovellia rubescens* n. sp., swimming cells, LM. **A–E**. Surface focus and optical sections of ventral views showing the cingulum displaced about one cingulum width and reddish bodies in the hypocone (thin arrows). The eyespot (e) is visible along the anterior part of the sulcus. The radiating arrangement of chloroplasts is discernible in B and D. The slight apical protrusion is visible in B and E (thick arrows). **F**. Dorsal (left) and lateral (right) views showing accumulation bodies in the epicone (arrowheads) and the transversely elongated nucleus (n) in the hypocone. Brownish granules are visible near the cell surface (asterisk). Scale bar = 10 μm. All to the same scale.

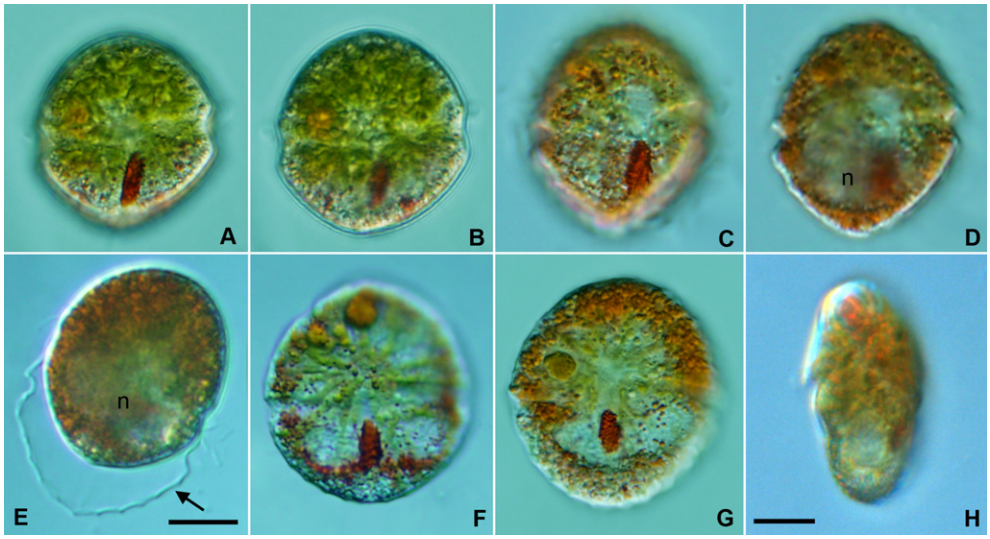

Figure 2 *Tovellia rubescens* n. sp., swimming cells in several stages of reddening, LM. **A**, **B**. Surface focus and optical section of a cell with reddish-brown granules in the hypocone. **C**, **D**. Surface focus and optical section of a cell with more numerous reddish-brown granules that mask the greenish colour of chloroplasts. In D, note the nucleus (n) extending to the cell centre and the cell surface somewhat wavy. **E**. Reddish-brown cell shedding the amphiesma through the anterior half, with the lower part somewhat denticulate (arrow). **F–H**. Ventral (F, G) and lateral (H) views of cells strongly compressed dorsoventrally, showing a round outline in ventral view and different amounts of reddish-brown granules in the cytoplasm. Scale bars = 10 μm. A–D, same scale as E; F and G, same scale as H.

determine with the available SEM images; it ranged roughly from twice to at least five times the width (Fig. 3D). About nine elongated plates bordered both sides of the ALP; they were four- or five-sided, 1.5–5.0 μm long and 0.5–1.5 μm wide (n = 38). The sulcal area contained four or five plates, arranged linearly (Fig. 3B). A ventral ridge (vr) was observed in the upper part of the sulcus, between the ends of the cingulum, partly covering the flagellar pores (Fig. 3A, B). Sutures between amphiesmal plates were sometimes raised on the hypocone, giving rise to a wavy or denticulate outline (Fig. 3B) reminiscent of the one seen in LM in some reddish cells (see above). Antapical plates did not differ significantly from other plates on the hypocone (Fig. 3E).

Cell ultrastructure (TEM)

General ultrastructural features are shown in Fig. 4A–6C. An approximately longitudinal section shows a postcingular, transversely elongated nucleus and chloroplast lobes radiating from a central pyrenoid to the cell surface (Fig. 4A, B). The chloroplast lobes were surrounded by three membranes and contained thylakoids in groups of three (Fig. 4D). The central pyrenoid extended irregularly into the chloroplast lobes and contained scattered thylakoid lamellae (Fig. 4B). In the epicone, the space between chloroplast lobes was mainly filled with oil droplets, whereas starch grains were the main storage material in the hypocone (Fig. 4A, B). Many vesicles bounded by a single membrane and containing numerous electron-opaque granules 20–50 nm in diameter were present between the central pyrenoid complex and the peripheral oil droplets, especially in the epicone (Fig. 4A–D). Scattered trichocysts were observed near the periphery and accumulation bodies were present near the pyrenoid (Fig. 4A, B). The pusular system is shown in Fig. 5A as a convoluted tube extending for about 10 μm from the flagellar insertion area. The tube was about 300 nm wide and was limited in stretches by a single membrane in direct contact with the cytoplasm (arrowheads in Fig. 5A, C), whereas in other zones it formed numerous diverticula closely enveloped by a surrounding vesicle, in a typical pusular configuration (arrows in Fig. 5A, B). The cell examined had accumulated a large number of oil droplets in the ventral area surrounding the sulcus, which made delimitation of the eyespot uncertain (not shown).

The flagellar base area of *T. rubescens* n. sp. is shown in serial sections in Fig. 6A–J, as seen from the ventral-right side and progressing away from the observer. A row of microtubules, accompanied by numerous electron-opaque vesicles, extended toward the protruding, electron-opaque structure called ventral ridge (vr), just anterior to the insertion position of the basal bodies (Fig. 6A, B). No connection was seen between any of the flagellar roots and this row of microtubules, which is interpreted as the microtubular strand of the peduncle (MSP), although an extended peduncle was not detected in any cell. Each flagellum was inserted in the cytoplasm within a depression lined by a single membrane; the opening to the exterior of these so-called flagellar canals was surrounded by a fibrous ring, known as the transverse and the longitudinal striated collars (TSC and LSC, respectively) (Fig. 6E, F). The basal bodies were roughly 400 nm apart and formed an angle of about 120°, as estimated from serial-section

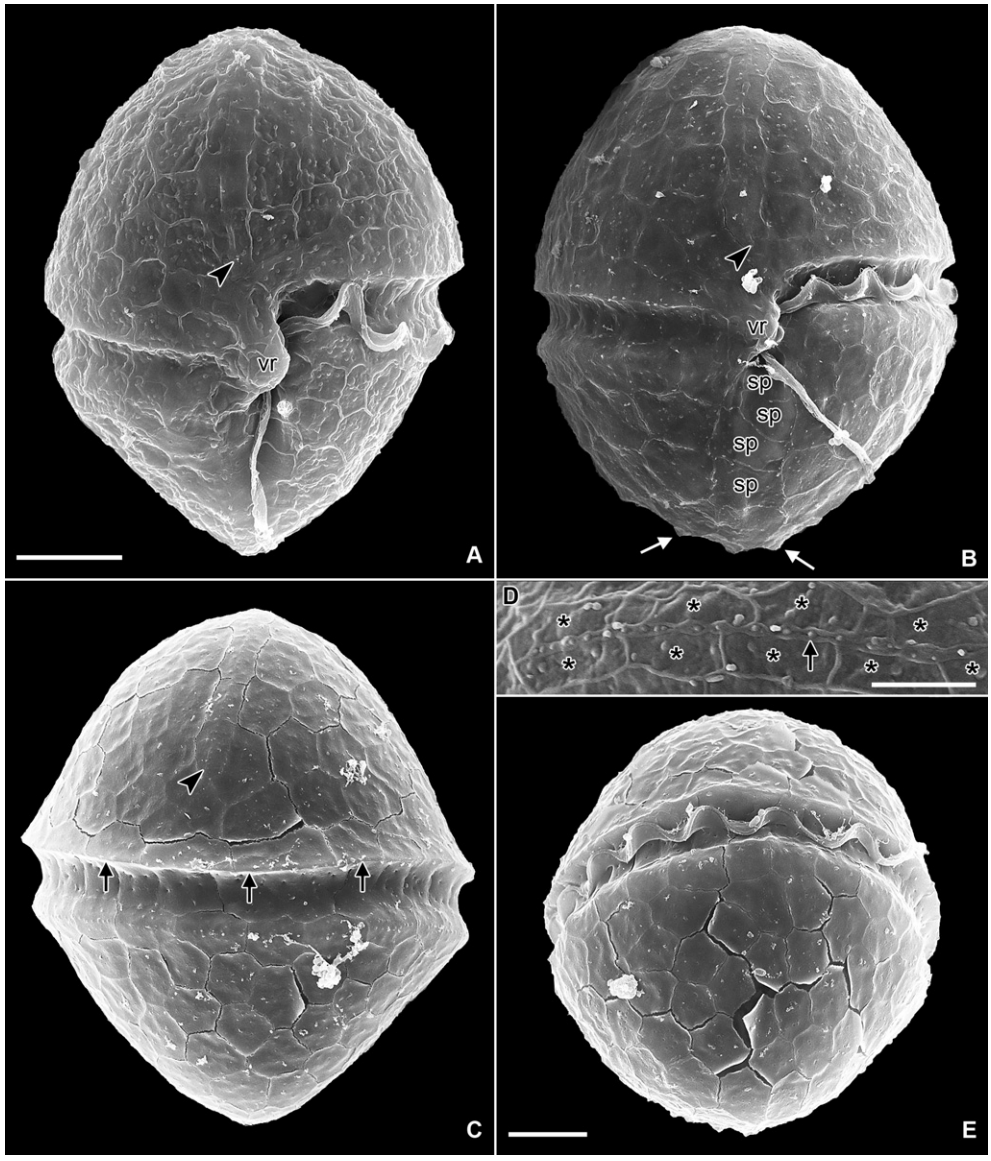

Figure 3 *Tovellia rubescens* n. sp., SEM. **A**, **B**. Ventral views, cell in A with smooth surface and conical hypocone, cell in B ellipsoid, with the hypocone somewhat denticulate in outline caused by a slight projection of the sutures (arrows). Four plates (sp) are disposed almost linearly along the sulcus. The arrowheads indicate the proximal end of the apical line of narrow plates (ALP). **C**. Dorsal view showing the distal end of the ALP (arrowhead) and the sharply delineated anterior border of the cingulum (arrows). **D**. Detail of the ALP composed by a row of very narrow plates with an axial row of knobs (arrow) and bordered by two rows of elongated plates (asterisks). **E**. Dorso-antapical view, showing the antapex. vr = ventral ridge. Scale bars: A = 5 μm; D = 2 μm; E = 5 μm. B and C, same scale as A.

observations. The longitudinal basal body (LB) associated on its proximal-left side with a strand of microtubules, the so-called longitudinal microtubular root or root 1 (LMR/r1). The proximal end of the LMR/r1 extended past the LB toward the ventral side for almost 1 μm (Fig. 6C–F). The proximal end of the transverse basal body (TB) was associated with two roots. The so-called transverse microtubular root, or root 3, (TMR/r3) started as a single microtubule closely following the anterior surface of the TB for some 300 nm before diverging gradually toward the anterior-left until it reached the surface of the flagellar canal; the TMR/r3 then sharply turned towards the cell apex, along a row of collared pits, and nucleated a series of about a dozen microtubules (Fig. 6F–J). The second microtubular root associated with the proximal end of the TB was a single microtubule closely connected to a striated fibre known as the transverse striated root (TSR; Fig. 6E–J); the microtubule is interpreted as root 4 (TSRM/r4). The TSR extended from the posterior surface of the TB toward the cell surface and ended near the TSC (Fig. 6I, J); on its proximal end, the TSR continued to the right, beyond the base of the TB, for over 500 nm (Fig. 6F). A distinctly

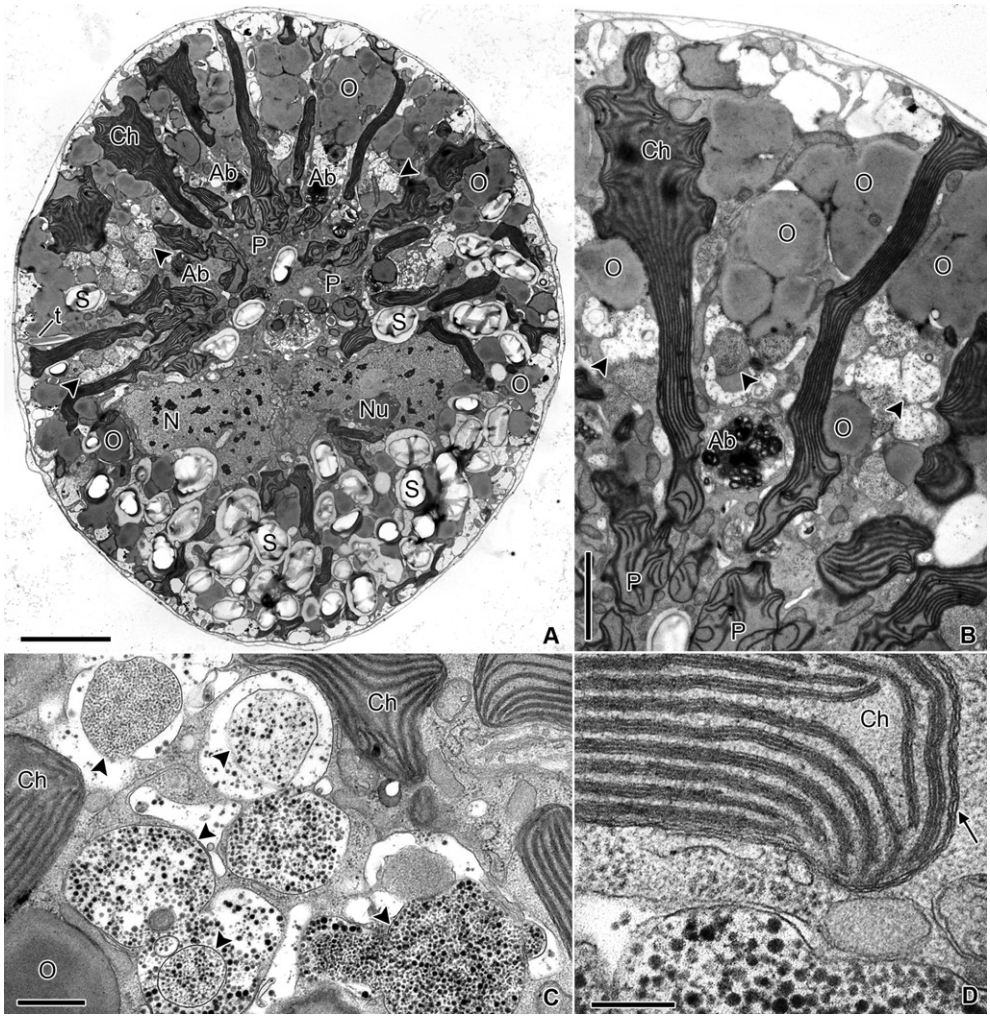

Figure 4 *Tovellia rubescens* n. sp., general ultrastructure, TEM. **A**. Longitudinal section of a cell seen from the ventral-right side showing the position of the nucleus (N) and the chloroplast lobes (Ch) radiating from a central compound pyrenoid (P). Numerous oil droplets (O) are visible in the epicone and starch grains (S) in the hypocone. Vesicles with numerous, small, electron-opaque granules are marked with arrowheads. **B**. Chloroplast lobes (Ch) intercalated with oil droplets and vesicles with electron-opaque granules (arrowheads). **C**. Vesicles with electron-opaque granules (arrowheads). **D**. Detail of a chloroplast lobe surrounded by three membranes (arrow) and part of a vesicle containing electron-opaque granules. Ab = accumulation body; nu = nucleolus; t = trichocyst. Scale bars: A = 5 μm; B = 2 μm; C = 500 nm; D = 200 nm.

striated fibrous component, the so-called striated root connective (SRC), linked the dorsal-anterior face of the LMR/r1 to the posterior side of the TSR (Fig. 6D–F).

Notes on the life cycle

Cells of *T. rubescens* n. sp. divided into two or four in the immobile stage (Fig. 7A–H). Before division, cells stopped, lost both flagella and rounded up, revealing a separate, outer layer. The nucleus of these division cysts then migrated towards the cell centre, where mitosis took place (Fig. 7A, B). Cytokinesis into two cells closely followed mitosis through the development of a cleavage furrow across the middle of the cell (Fig. 7B). Cytokinesis into four cells seemed to be a one-step process in which cleavage furrows extended inward from the periphery, separating four cells in a tetrahedral arrangement (Fig. 7C–E). Offspring cells slowly emerged from the division cyst following the rupture of its surface layer and started swimming, usually within a few minutes (Fig. 7F–H); the flagella, especially the longitudinal, were sometimes noted already inside the cyst. After being released from division cysts most cells grew for several days until they eventually divided again.

Attempts to induce sexual reproduction were generally unsuccessful. A minority of small cells eventually appeared in all batches, whether in single culture lines grown in full growth medium, or in single or mixed culture lines grown in full, N-deficient or P-deficient medium. However, groups of small cells swimming around one another (the "dancing groups" of Stosch 1973) were never observed and the origin of pairs of connected cells

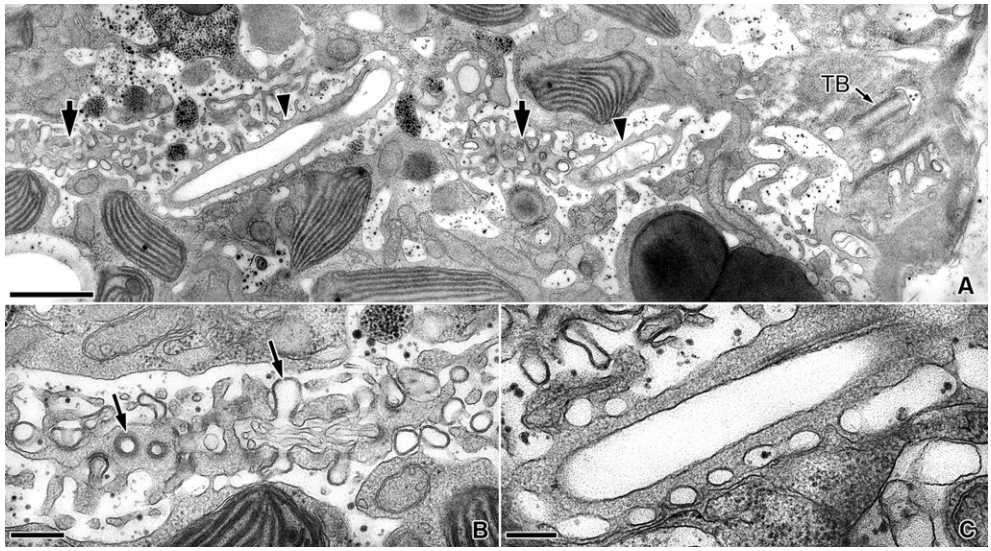

Figure 5 *Tovellia rubescens* n. sp., pusular system, TEM. **A**. Sections through the pusular tube, some showing diverticula (short arrows) and others showing the tube lined by a single membrane (arrowheads). The flagellar base area is marked on the right side of the image by the transverse basal body (TB). **B**. Transverse and longitudinal sections through diverticula of the pusular tube (arrows). **C**. Portion of pusular tube lined by a single membrane. Scale bars: A = 1 μm; B = 300 nm; C = 200 nm.

that appeared in the batches is uncertain. Cells in these pairs were connected by the epicones (Fig. 8A) or by their dorso-lateral sides (Fig. 8B). Repeated observations of such paired cells isolated into separate culture-plate wells showed progressive fusion, suggesting they were in fact fusing gametes. However, the putative fusion was never observed to yield regular planozygotes; instead, cells kept an abnormal aspect, with the longitudinal flagella emerging from different, sometimes distant positions in the cell (not shown). To confuse matters further, similar cells were seen exiting from immobile stages reminiscent of division cysts. Whatever their origin, these "double-cell" forms swam for several days and eventually died, leaving their significance uncertain. Ellipsoid or ovoid brownish-red cells without flagella and with a smooth wall-like cover appeared in low numbers in old batches and in cultures grown in N-deficient and P-deficient medium (Fig. 8C). These cyst-like cells were repeatedly observed on the bottom of culture wells and their contents were seen to degrade soon, rendering further observations unfeasible. Fully formed resistance cells were never found in the cultures. Resting cysts resembling these cyst-like cells in general shape and contents were collected several times from the pond where the original strain of *T. rubescens* n. sp. originated. However, contrary to the smooth surface of walled cells formed in culture, cysts collected from the field had 2.5–5.0-μm long spines with pointed or sometimes branched tips (Fig. 8D–F). On the basis of ITS sequences determined from field-collected cysts with the described morphology, these resting cells were interpreted as belonging to *T. rubescens* n. sp. Field-collected cysts isolated into full medium germinated after 4–6 d, giving rise to swimming cells with *T. rubescens* n. sp. morphology, also with reddish bodies in the hypocone. However, these cells divided, at most, a few times and did not produce viable cultures.

Colour changes and pigment analyses

The acquisition of a reddish tinge occurred gradually in cells as batches grown in full medium approached the lag phase. Although distinct at the cell level, colouration of batches was very slight, manifesting mostly in reddish-brown deposits on the bottom of culture bottles. In N-deficient and P-deficient media, the reddening developed sooner and was visible in most cells of 10-d old batches. The final cell densities obtained in incomplete media, quite lower than in full medium, along with the shorter exponential growth phase, made direct comparisons of pigment concentrations unreliable. In addition, differences in cell size, which tended to be more irregular, but generally smaller in incomplete media, precludes any attempt to normalize results based on the number of cells extracted. The pigments detected in extracts from batches of *T. rubescens* n. sp. grown in full and in N-deficient medium, and of *T. aveirensis* grown in similar conditions are shown in Table 1. The results in Table 1 are not quantitative, both in the sense that concentrations cannot be inferred from these data and in that direct comparisons across columns are not valid. However, the relative values associated with the detection intensities are a rough indication of proportions between pigments detected in a particular batch. Also, only the more abundant species were identified by MS/MS, while less abundant species were only identified by their molecular weight. The photosynthetic apparatus pigments identified were standard for

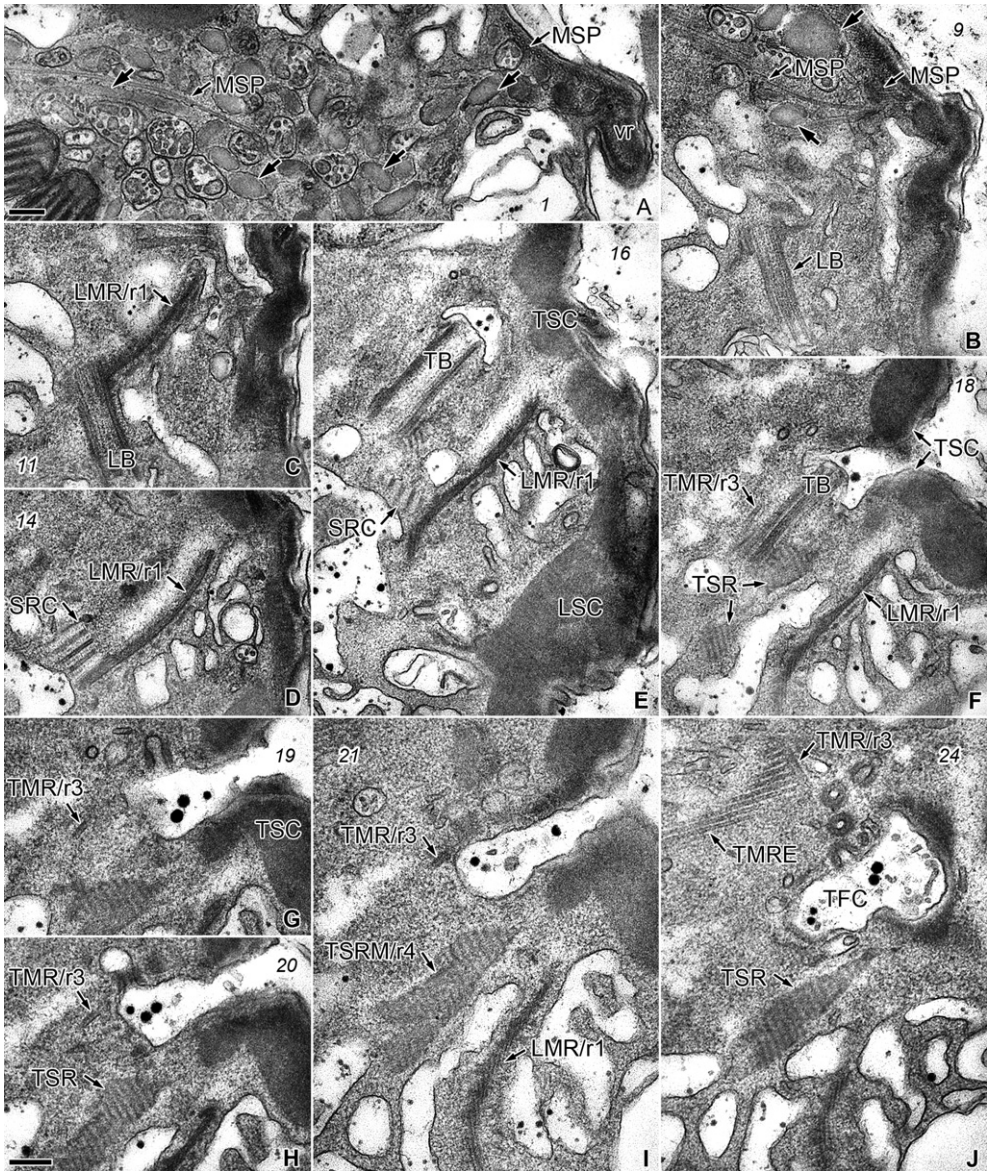

Figure 6 *Tovellia rubescens* n. sp., flagellar apparatus, TEM. Nonadjacent serial sections viewed approximately from the ventral-right side of the cell and progressing away from the observer. Small slanted numbers represent section number. **A**, **B**. The microtubular strand of the peduncle (MSP) and accompanying electron-opaque vesicles (arrows) converge to the ventral area, near the ventral ridge (vr). **C**–**F**. The relatively long and straight proximal part of the longitudinal microtubular root (LMR/r1) contacts the longitudinal basal body (LB) in C, and the striated root connective (SRC) in D. In E, the SRC reaches the transverse striated root (TSR). The transverse microtubular root (TMR/r3) is marked in F, near the anterior surface of the TB. **G**–**J**. The TMR/r3 extends towards a row of collared pits at the surface of the transverse flagellar canal (TFC), turns upward and nucleates a row of microtubules (transverse microtubular root extension, TMRE; marked in J). The TSR and its associated microtubule (TSRM/r4) extend towards the cell surface, near the transverse striated collar (TSC). LSC, longitudinal striated collar. Scale bars = 200 nm. B–E, same scale as A. F, G, I and J, same scale as H.

peridinin-containing dinoflagellates. Astaxanthin and several compounds related to astaxanthin metabolism (adonirubin, astacene, astaxanthin monoesters) were unequivocally identified in *T. rubescens* n. sp., both in full-medium and in N-deficient-medium grown batches. Astaxanthin, two of its monoesters and astacene were also present in *T. aveirensis*, although neither the cells nor the extract showed a red tinge.

Phylogeny of *Tovellia rubescens* n. sp

The *Tovellia* species included in alignment 1, based on partial LSU rDNA sequences, formed a single clade with maximum statistical support (Fig. 9). *Tovellia rubescens* n. sp. formed a highly supported sister taxon to *T. aveirensis* and *T.* cf. *aveirensis* (posterior probability = 1, bootstrap support = 100%). *Tovellia sanguinea* and *T. coronata*

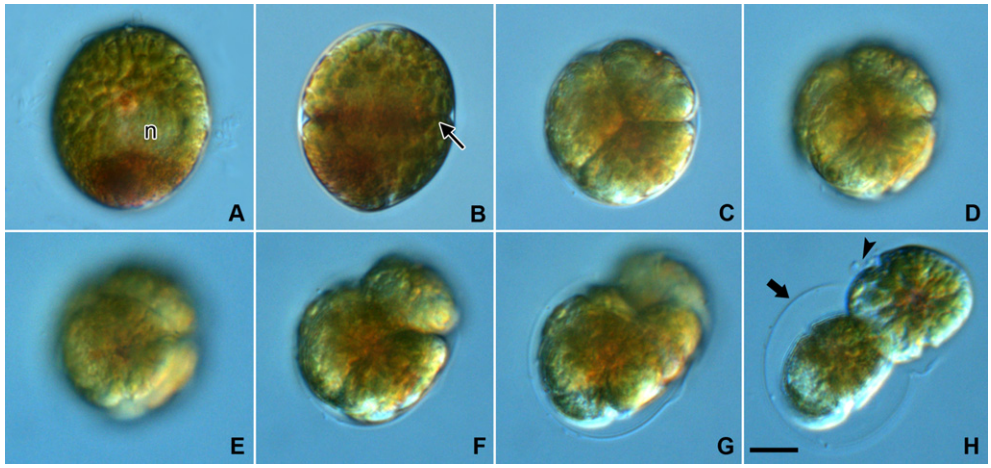

Figure 7 *Tovellia rubescens* n. sp., cell division, LM. **A**, **B**. Stages during division into two cells. The cell lost mobility and the nucleus (n) migrated to the cell centre (A). Cytokinesis occurs through the formation of a cleavage furrow (thin arrow in B). **C**–**E**. Division cyst with four cells in tetrahedral arrangement (different focal levels). **F**–**H**. Release of daughter cells following the rupture of the enveloping layers of the cyst (thick arrow). The transverse flagellum of one cell is perceptible (arrowhead in H). Scale bar = 10 μm. All to the same scale.

(Wołoszyńska) Moestrup, K. Lindberg and Daugbjerg (both species with red cells) appear in the Bayesian tree (Fig. 9) as the nearest relatives to *T. rubescens* n. sp. and *T. aveirensis* with lower statistical support. *Tovellia rinoi* formed the earliest divergent lineage among the *Tovellia* species included in alignment 1 (Fig. 9). The analysis did not clarify the closest relative to the Tovelliaceae because the deep branches formed a polytomy (Fig. 9).

The analysis of alignment 2, including only the Tovelliaceae present in alignment 1 with the addition of *Tovellia diexiensis*, again displays *T. rubescens* n. sp. as a sister taxon to *T. aveirensis* and *T.* cf. *aveirensis* with the highest statistical support (Fig. 10). *Tovellia diexiensis* and *T. sanguinea* form a clade with high posterior probability (pp = 1), but poor bootstrap support (bs = 75%). *Tovellia coronata*, the *T. sanguinea/T. diexiensis* clade and the *T. rubescens* n. sp./*T. aveirensis* clade formed a polytomy (i.e. no statistical support for the tree topology) (Fig. 10).

DISCUSSION

Taxonomic affinities of *T. rubescens* n. sp

Motile cells of *T. rubescens* n. sp. showed a combination of morphological features typical of Tovelliaceae, including a tubular pusule with diverticula (see Calado 2011; Calado et al. 2006), an extraplastidial eyespot of type C (Moestrup and Daugbjerg 2007), an amphiesma made of numerous vesicles with thin plates roughly arranged in latitudinal series, and the general arrangement of basal bodies and flagellar roots (see below). The presence of an ALP sensu Lindberg et al. (2005) surrounded by two rows of narrow apical plates places the new species in *Tovellia*. The taxonomic affinity with other *Tovellia* species is also unequivocally supported by LSU rDNA-based analyses, which mark *T. aveirensis* as the closest known relative of *T. rubescens* n. sp.

Morphological comparisons between described species of *Tovellia* have been summarized in Pandeirada et al. (2014), Li et al. (2015) and Zhang et al. (2016); a further species, *T. rinoi*, was described after the publication of these articles (Pandeirada et al. 2017). *Tovellia rubescens* n. sp. cells showed a wide range of sizes, which reduces the value of cell dimensions as a feature for distinction from other species. In contrast, plate arrangement, with 12–15 latitudinal series of plates (including two series in the cingulum) separates *T. rubescens* n. sp. from *T. coronata*, *T. diexiensis*, *T. glabra* (Wołoszyńska) Moestrup, K. Lindberg and Daugbjerg, *T. nygaardii* Moestrup, K. Lindberg and Daugbjerg, *T. paldangensis* Zhun Li, M. S. Han and H. H. Shin, *T. rinoi* and *T. sanguinea*, none of which exceed 10 latitudinal series; and from *Tovellia stoschii* (Shyam and Sarma) Moestrup, K. Lindberg and Daugbjerg, which has about 17 latitudinal series of relatively small plates (Christen 1958; Li et al. 2015; Lindberg et al. 2005; Moestrup et al. 2006; Shyam and Sarma 1976; Wołoszyńska 1917; Zhang et al. 2016). *Tovellia apiculata* (Stosch) Moestrup, K. Lindberg and Daugbjerg, *T. aveirensis* and *T. leopoliensis* (Wołoszyńska) Moestrup, K. Lindberg and Daugbjerg have numbers of latitudinal plate series similar to *T. rubescens* n. sp., but show other differences. Motile cells of *T. leopoliensis* are strongly flattened dorsoventrally, making it very distinctive within the genus (Moestrup and Calado 2018; Wołoszyńska 1917). Vegetative cells of *T. aveirensis* are more smoothly rounded than *T. rubescens* n. sp., especially on the hypocone, which rarely is slightly pointed; the ALP of *T. aveirensis* is shorter on the dorsal side (Pandeirada et al. 2014), with up to five plates separating its dorsal end from the cingulum, versus two (rarely three) plates in *T. rubescens* n. sp. The cell shape of *T. rubescens* n. sp. resembles that of *T. apiculata*, except for the antapical "apiculus," made by three to four plates, that justifies the latter species' name (Stosch 1973). The cyst described for

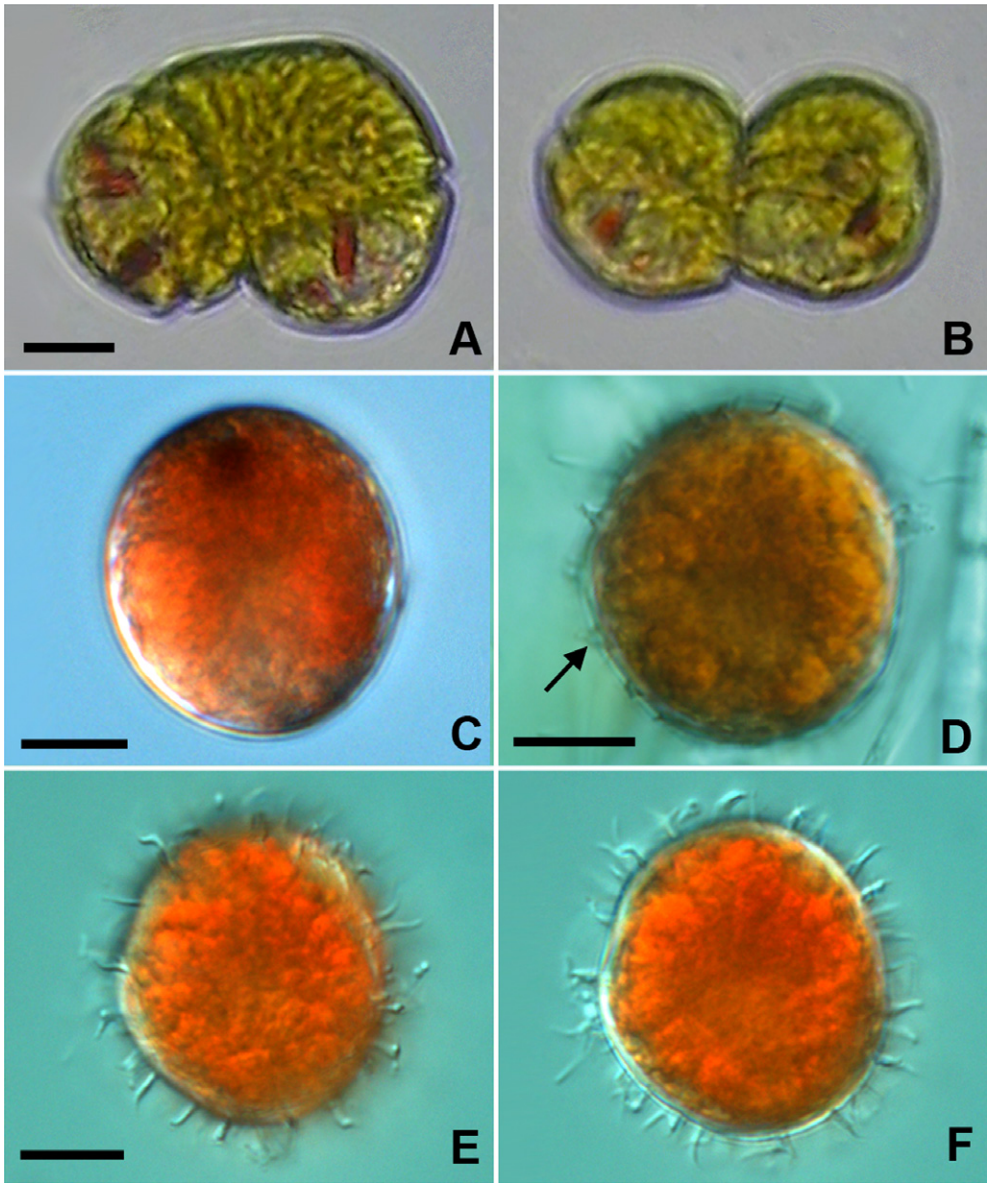

Figure 8 *Tovellia rubescens* n. sp., paired cells of uncertain significance, and resting stages, LM. **A**, **B**. Cells connected by the epicones and by their dorsal-lateral sides, respectively. **C**. A nonmotile, brownish-red cell from culture. **D–F**. Field-collected cysts with ornamented walls. Scale bars = 10 μm. A and B, same scale. E and F, same scale.

T. apiculata also showed a sharp antapical projection and was of the *T. coronata* type, that is, somewhat projected along the axis and with two latitudinal rings of protuberances, one anterior and one posterior to an equatorial constriction (Stosch 1973). In contrast, the field-collected red cysts with an ITS rDNA sequence identical to motile cells of *T. rubescens* n. sp. did not show a marked paracingulum and were covered by evenly distributed spines. This general morphology appears closer to the cysts of *T. aveirensis*, which, however, showed a marked paracingulum and spines twice as long when mature; and, to some extent, to cysts of *T. paldangensis*, which had much fewer and shorter spines (Moestrup and Calado 2018; Pandeirada et al. 2014). The presence of a cyst of the same general type was the justification for the recent transfer of *T. dodgei* (Sarma and Shyam) K. N. Mertens and H. Gu from the genus *Gymnodinium* (Luo et al. 2016; Sarma and Shyam 1974). The cysts of *T. dodgei* were also red, but the motile cells were more elongate and the sulcus invaded the epicone, creating a distinct plough-shaped depression. The chloroplasts of *T. dodgei* were described as discoid, whereas radiating chloroplast lobes were visible in *T. rubescens* n. sp., even in LM. The organization of the amphiesmal plates of *T. dodgei* was not described (Moestrup and Calado 2018; Sarma and Shyam 1974). A sequence divergence was estimated to evaluate the

Table 1. Pigments identified by HPLC-MS/MS in extracts from *Tovellia rubescens* n. sp. and *Tovellia aveirensis* culture batches grown with and without a nitrogen (N) source

		T. rubescens[a]		*T. aveirensis*[a]	
Pigment	*m/z* ([M+H]$^+$)	With N	Without N	With N	Without N
Adonirubin	581.4	1.3×10^4	2×10^4	nd	nd
Astaxanthin	597.4	1.4×10^5	3.2×10^4	3.8×10^5	1.5×10^4
Astx monoester 14:0	807.6	8.4×10^4	7.8×10^4	Vest	Vest
Astx monoester 16:0	835.6	1.5×10^5	1.3×10^5	1.7×10^4	nd
Astx monoester 16:4	829.6	9.3×10^3	3.3×10^4	4.0×10^4	nd
Astx monoester 18:0	863.7	3.1×10^4	4.0×10^4	nd	nd
Astx monoester 18:1	861.6	1.0×10^4	3.8×10^3	nd	nd
Astacene	593.4	4.0×10^4	1.7×10^4	1.8×10^4	nd
Canthaxanthin	565.4	3.2×10^4	nd	nd	nd
Chlorophyll a	893.5	5.1×10^3	nd	nd	nd
Chlorophyll c2	609.2	1.7×10^4	nd	nd	nd
Diadinoxanthin	583.4	2.0×10^5	8.0×10^4	4.6×10^4	5.3×10^4
Dinoxanthin	643.4	3.4×10^4	9.4×10^3	7.0×10^4	2.5×10^4
Peridinin	631.4	2.7×10^4	2.7×10^4	1.0×10^4	8.4×10^3
β-Carotene	537.4	2.0×10^4	5.6×10^3	nd	nd

nd = No detection; Vest = vestigial.

The approximate number of cells used for pigment extraction was: 108,000 for both growth conditions of *T. rubescens* n. sp.; 68,900 cells of *T. aveirensis* grown in N-deficient medium, and 133,800 grown in full medium.

[a]Relative abundance of the molecular ion of the pigment, in counts, from cells grown with and without a source of nitrogen (N).

molecular support for a species delineation between the closely related *T. rubescens* n. sp. and *T. aveirensis*. Using the Kimura-2-parameter model and 1,344 aligned base pairs of the LSU rDNA (including domain D2) the divergence estimate was 3.9%. Despite some overlap in morphology, this divergence indicates two distinct species.

Cell ultrastructure

The arrangement of flagellar bases and roots observed in one cell of *T. rubescens* n. sp. closely matched what has been described from other members of the Tovelliaceae, particularly the relative positioning of the basal bodies, with the nearly 400-nm distance between their proximal ends highlighted by the large SRC and its connection to the proximal part of the TSR (see summary of tovelliacean characters in Calado 2011). The nearly straight proximal part of the LMR/r1 that projects ventrally past the LB is another feature in common with species of Tovelliaceae for which the disposition of flagellar roots is known in enough detail (Calado 2011; Calado et al. 2006; Roberts and Timpano 1989; Roberts et al. 1995). The arrangement of roots and connectives near the flagellar bases is consistently different in species of Peridiniales, in which the SRC is replaced by a much wider layered connective, which spans a rather shorter distance between the TSR and a fibrous layer on the dorsal face of the LMR/r1 (Calado et al. 1999; Craveiro et al. 2009, 2013, 2015). Where known, species of Gonyaulacales and Suessiales have the dorsal side of the LMR/r1 linked to a more distal area of the TSR by a narrow SRC and, like the Peridiniales, have a curved proximal end of LMR/r1 barely projecting beyond the LB (Craveiro et al. 2010; Hansen and Moestrup 1998; Jeong et al. 2014; Roberts 1989).

The radial chloroplast lobes associated with a central pyrenoid complex observed in *T. rubescens* n. sp. match the chloroplast arrangement of the closely related *T. sanguinea* and *T. aveirensis* (Moestrup et al. 2006; Pandeirada et al. 2014). In contrast, *T. coronata* did not display a central pyrenoid complex (Lindberg et al. 2005). The recently described *T. diexiensis*, which appears as a close relative of *T. sanguinea* in LSU rDNA-based phylogenies, was reported to have small, parietal chloroplasts that were often difficult to discern due to the presence of numerous red bodies (Zhang et al. 2016). The reported absence of a central pyrenoid complex in *T. diexiensis* suggests an unexpected lability in the plastidome of this group of species. The observation by LM of the radial arrangement of chloroplast lobes can be remarkably difficult even in cells larger than *T. diexiensis* (Craveiro et al. 2009); whether a central pyrenoid complex may have passed undetected during epifluorescence observations is, however, unclear.

A row of microtubules accompanied by vesicles with electron-opaque contents, interpretable as an MSP, similar to the ones shown here for *T. rubescens* n. sp. and in Moestrup et al. (2006) for *T. sanguinea*, has been found in all species of *Tovellia* that have been examined by TEM (Moestrup et al. 2006, p. 59 concerning *T. coronata*; unpublished observations on *T. aveirensis*). Although observations on the MSP of species of *Tovellia* resemble what was demonstrated from predatory species with feeding mechanisms involving similar microtubular strands

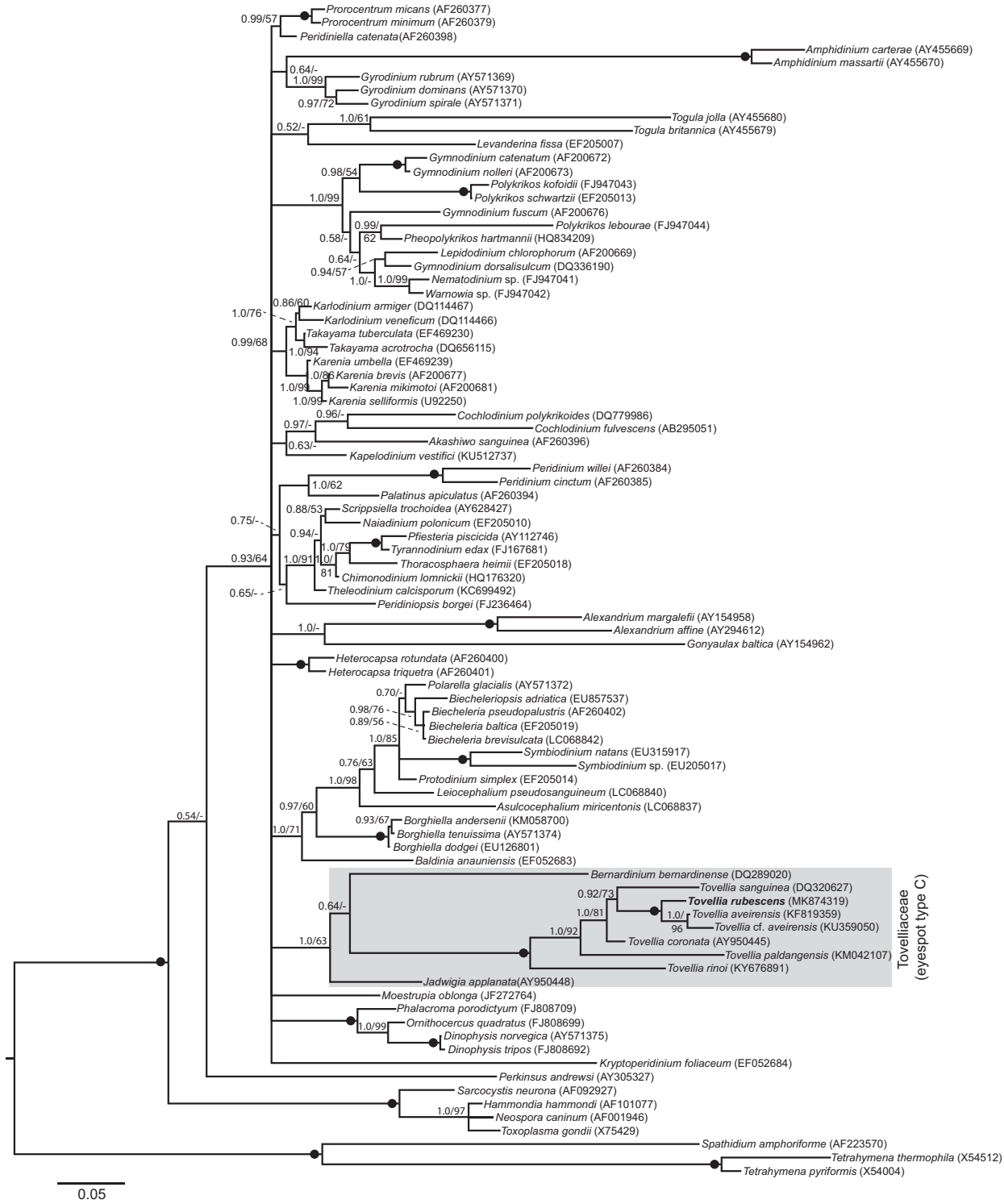

Figure 9 Phylogeny of *Tovellia rubescens* n. sp. based on nuclear-encoded LSU rDNA (1,151 base pairs) and analysed with Bayesian inference. The ingroup of dinoflagellates was polarized using ciliates (three species), apicomplexan (four species) and a perkinsozoan. Numbers to the left of slashes at internal nodes are posterior probabilities (≥ 0.5) from Bayesian analysis followed by bootstrap values (≥ 50%) from maximum likelihood with 1,000 replications. Bootstrap values < 50% are indicated by a "-". Filled circles replace numbers when statistical support was the highest possible for both Bayesian and maximum likelihood analyses (1.0 and 100%, respectively). GenBank accession numbers are added in parentheses. Dinoflagellates with type C eyespot sensu Moestrup and Daugbjerg (2007), corresponding to the family Tovelliaceae, are marked by a rectangle. Branch lengths are proportional to the number of character changes.

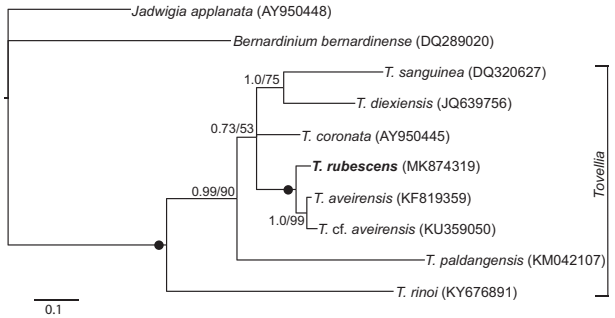

Figure 10 Phylogeny of *Tovellia rubescens* n. sp. and six other well circumscribed species of *Tovellia* based on 714 base pairs (including domain D1–D2) and analysed with Bayesian inference. *Jadwigia* formed the outgroup taxon. Numbers to the left of slashes at internal nodes are posterior probabilities (≥ 0.5) from Bayesian analysis followed by bootstrap values (≥ 50%) from maximum likelihood with 1,000 replications. Filled circles represent maximum support. GenBank accession numbers are written in parentheses and branch lengths are proportional to the number of character changes.

and vesicles (Calado et al. 1998, 2006), direct evidence of mixotrophy in the genus has not been reported.

The abundant oil droplets found between chloroplast lobes in a red cell of *T. rubescens* n. sp. are reminiscent of the oil bodies interpreted as the location of accumulated astaxanthin-related compounds in cells of green algae associated with red snow (Remias et al. 2016) and in species of the industrially important genera *Chlorella* Beijerinck and *Haematococcus* Flotow (Bar et al. 1995; Mulders et al. 2015; Santos and Mesquita 1984; Solovchenko 2015). Although apparently more localized in the cell, the pigment aggregates documented by TEM in *T. sanguinea* also displayed the roundish outline of lipid globules, suggesting the oil droplets of *T. rubescens* n. sp. as the likely structures where reddish pigments accumulate in this species (Moestrup et al. 2006). The significance of the numerous vesicles containing electron-opaque globules is unknown.

Life cycle

The mechanism of vegetative cell multiplication observed in *T. rubescens* n. sp. falls within the typical pattern established from other *Tovellia* species, in which 2–8 offspring cells are produced in a temporary, or division, cyst (Christen 1958; Pandeirada et al. 2014, 2017; Shyam and Sarma 1976; Stosch 1973; Wołoszyńska 1917; Zhang et al. 2016). However, contrary to what is known from other species of *Tovellia*, *T. dodgei* cells were reported to divide in the swimming stage (Sarma and Shyam 1974). Examination of *T. dodgei* by modern methods, including the clarification of amphiesmal features and molecular analysis, is necessary to establish its relationship with species of Tovelliaceae (Pandeirada et al. 2017).

The production of resting cysts as one of the possible outcomes of sexual reproduction is well established in the genus *Tovellia* (Pandeirada et al. 2017; Stosch 1973). The finding in the same pond of swimming cells of *T. rubescens* n. sp. and resting cysts with an identical ITS1-5.8S-ITS2 rDNA sequence suggests the occurrence of sexual reproduction in wild populations of the species. The lack of successful gamete fusion and viable resting cyst formation in culture batches maintained in the same conditions under which sexually reproducing strains of *T. aveirensis* and *T. rinoi* were observed may be explained by heterothally of the strains available (Pandeirada et al. 2014, 2017). Mixing the two available lines of *T. rubescens* n. sp. did not result in detectable sexual reproduction indicating sexual incompatibility. Likewise, no signs of sexual reproduction were detected in experimental mixtures of *T. rubescens* n. sp. with available strains of *T. aveirensis*.

The occurrence in the culture batches of distinctly flattened cells that appeared strikingly different from the more common globose cells, with no intermediate morphologies, is noteworthy. The regular formation of small numbers of these cells in batches started by re-isolation of single cells of the cultures excluded the possibility that they originated from a contamination. We were not able to link the flat cells to any particular life cycle stage, nor to any particular function in the culture batches. A recent discussion on the significance of flattened cells appearing in cultures of *Protoceratium reticulatum* (Claparède and J. Lachmann) Buetschli and *Ceratocorys mariaovidiorum* P. Salgado, S. Fraga, F. Rodríguez, Riobó and I. Bravo suggests a link to a benthic stage of these species, arguably because flat cells would be better adapted to move in the interstitial environment of the sediment, or to attach to sediment particles (Salgado et al. 2018). Whether benthic flattened cells of *T. rubescens* n. sp. occur in the shallow ponds where the species was found is currently unknown.

Colour changes and pigment composition

The observed switch from a general yellowish-green colour of cells of *T. rubescens* n. sp. in culture batches during early exponential growth to a distinctly reddish-brown colour as batches approached the terminal lag phase suggests that the accumulation of red pigment is a response to stress. The more rapid induction of the reddish-brown colour in batches grown in N- or P-deficient medium points to nutrient deficiency as a trigger for the increase in red pigment concentration in the cells. Stress conditions, such as nutrient starvation or high light intensity, are among the standard methods for the induction of astaxanthin accumulation in mass cultures of industrially important producers of this antioxidant, green algae of the genera *Chlorella* and *Haematococcus* (Bar et al. 1995; Fábregas et al. 1998; Mulders et al. 2015).

Although astaxanthin has been reported from very few dinoflagellates, the abundance of astaxanthin and its esters in some red species of *Tovellia* is well documented (Frassanito et al. 2005; Zhang et al. 2016; see Frassanito et al. 2006 for earlier records of astaxanthin-related carotenoids in dinoflagellates). The finding of adonirubin and

canthaxanthin in extracts of *T. rubescens* n. sp., and the absence of beta-cryptoxanthin, zeanxanthin and adonixanthin suggest the pathway of astaxanthin biosynthesis that involves the enzyme beta-carotene ketolase (Han et al. 2013). The pigment analysis performed in the present work was expected to reveal the changes in pigment composition that determine the reddening of the cells of *T. rubescens* n. sp., namely through a marked increase in proportion of some of the red compounds relative to other pigments. However, the results of the analyses, summarized in Table 1, do not provide a clear explanation for the observed increase of the reddish-brown colour in cells of older or nutrient-depleted batches. It has been shown that the later stages of astaxanthin accumulation in *Haematococcus* and several other green algae mainly involve diesters of astaxanthin (Orosa et al. 2001) and astaxanthin diesters were identified in *T. sanguinea* and *T. diexiensis* (Frassanito et al. 2006; Zhang et al. 2016). However, the analyses reported herein for *T. rubescens* n. sp. were limited to a maximum range of *m/z* 1,000, leaving astaxanthin diesters out of range and rendering their participation in cell reddening in this species as speculative.

The inability of culture batches of *Tovellia aveirensis* to acquire a reddish colour, even when submitted to the same treatments that never failed to elicit the reddening of *T. rubescens* n. sp., was one of the earliest noted constant differences between the two species. Therefore, the detection of astaxanthin and astaxanthin monoesters in *T. aveirensis* came as a surprise. However, batches of *T. aveirensis* fared more poorly under nutrient stress than those of *T. rubescens* n. sp., and the overall amount of astaxanthin showed no signs of increasing, suggesting that a response to stress through activation of astaxanthin-related metabolic pathways is either reduced or absent in *T. aveirensis*. The presence of astaxanthin-related metabolism in *T. aveirensis* is coherent with its well-established phylogenetic relationship to a group of species in which reddish colouration has been linked to the accumulation of astaxanthin metabolites. In this context, the reported absence of astaxanthin in the phylogenetically related *T. coronata*, which also displays a red colour, is difficult to explain (Lindberg et al. 2005). Perhaps re-examination of the pigment composition of *T. coronata* using a combination of HPLC and mass spectroscopy would be justified to clarify the presence or absence of astaxanthin in this species.

TAXONOMIC SUMMARY

Meeting the requirements of the ICN 2018 (Turland et al. 2018).
Supergroup Alveolata [informal; based on Cavalier-Smith (1991), as infrakingdom]
Phylum Dinoflagellata Fensome et al. 1993
Class Dinophyceae F. E. Fritsch 1927
Order Tovelliales Moestrup and Calado 2018
Family Tovelliaceae Moestrup, K. Lindberg and Daugbjerg 2005
Genus *Tovellia* Moestrup, K. Lindberg and Daugbjerg 2005

Tovellia rubescens Pandeirada, Craveiro, Daugbjerg, Moestrup and Calado n. sp.

Description. Epicone nearly hemispherical and hypocone hemispherical to rounded conical, sometimes with a pointed antapex. Epicone occasionally projected at the level of the ALP. Cingulum descending, displaced about one cingulum width, epi- and hypocone of similar size. Most cells slightly compressed dorsoventrally, with hypocone somewhat flattened obliquely in lateral view, 18.5–43 μm long, 12.5–33 μm wide and 11.5–28 μm thick. Chloroplasts yellowish-green, with lobes radiating from a central pyrenoid complex. Eyespot red, extraplastidial, located along the sulcal area. Transversely elongated nucleus in the dorsal part of the hypocone. Accumulation bodies predominantly in the epicone, and small, rounded reddish-brown bodies in the hypocone. Vegetative cells changing from yellowish-green to reddish-brown in response to stress conditions. Some reddish-brown cells almost circular in ventral view and strongly compressed dorsoventrally. Amphiesma with numerous pentagonal or hexagonal vesicles containing thin plates, roughly disposed along six latitudinal series on the epicone and four or five series on the hypocone; cingulum with two series of plates, those of the anterior series rectangular or pentagonal and sharply defining the anterior edge of the cingulum, plates of the posterior series roughly hexagonal and extending onto the hypocone, over the rounded posterior cingulum edge. A line of narrow plates (ALP) extends over the apex of the cell, from nearly above the sulcus, about one plate away from the proximal end of the cingulum, to the dorsal side, two or three rows of plates from the anterior cingulum edge. Astaxanthin and metabolically related pigments present. Asexual division into two or four cells, by means of division cysts. Ellipsoid to ovoid brownish-red cysts without a marked paracingulum, with the wall provided with evenly distributed 2.5–5 μm long spines with pointed or branched tips.
Holotype. SEM stub with critical point-dried cells from MSP1 culture line deposited at the University of Aveiro Herbarium, registered as AVE-A-T-8. Fig. 3A–E show cells from this stub.
Type locality. Freshwater lake in Gafanha da Boavista, Ílhavo, Portugal (40°35′44.70″N, 8°41′49.66″W), sampled on 28 October 2010.
Etymology. Epithet from Latin *rubescens*, turning red, reddening.
Gene sequence. LSU rDNA sequence for *T. rubescens* deposited in GenBank with the accession number MK874319; the ITS1-5.8S-ITS2 rDNA sequence has the accession number MK874823.
Zoobank registration number. urn:lsid:zoobank.org:act:165E6F44-1A0E-44DE-91C9-0D662833FA00.

ACKNOWLEDGMENTS

MSP and SCC were supported respectively by grants SFRH/BD/109016/2015 and SFRH/BPD/68537/2010 from the financing programs POCH – Programa Operacional

Capital Humano and QREN – POPH – Tipologia 4.1 – Formação Avançada, and by the European Social Funding (FSE) and the Portuguese Ministry of Education and Science (MEC). GeoBioTec (UID/GEO/04035/2013) supported this project. The molecular work was done in the facilities at the Laboratory of Molecular Studies for Marine Environments (LEMAM), Univ. Aveiro, Portugal. Thanks are due for the financial support to QOPNA (FCT UID/QUI/00062/2019) and Portuguese Mass Spectrometry Network (LISBOA-01-0145-FEDER-402-022125) to FCT/MCTES through national funds (PIDDAC), and the co-funding by the FEDER, within the PT2020 Partnership Agreement and Compete 2020.

LITERATURE CITED

Bar, E., Rise, M., Vishkautsan, M. & Arada, S. M. 1995. Pigment and structural changes in *Chlorella zofingiensis* upon light and nitrogen stress. *J. Plant Physiol.*, 146:527–534.

Calado, A. J. 2011. On the identity of the freshwater dinoflagellate *Glenodinium edax*, with a discussion on the genera *Tyrannodinium* and *Katodinium*, and the description of *Opisthoaulax* gen. nov. *Phycologia*, 50:641–649.

Calado, A. J., Craveiro, S. C., Daugbjerg, N. & Moestrup, Ø. 2006. Ultrastructure and LSU rDNA-based phylogeny of *Esoptrodinium gemma* (Dinophyceae), with notes on feeding behavior and the description of the flagellar base area of a planozygote. *J. Phycol.*, 42:434–452.

Calado, A. J., Craveiro, S. C. & Moestrup, Ø. 1998. Taxonomy and ultrastructure of a freshwater, heterotrophic *Amphidinium* (Dinophyceae) that feeds on unicellular protists. *J. Phycol.*, 34:536–554.

Calado, A. J., Hansen, G. & Moestrup, Ø. 1999. Architecture of the flagellar apparatus and related structures in the type species of *Peridinium*, *P. cinctum* (Dinophyceae). *Eur. J. Phycol.*, 34:179–191.

Cavalier-Smith, T. 1991. Cell diversification in heterotrophic flagellates. *In:* Patterson, D. J. & Larsen, J. (ed.), The Biology of Free-living Heterotrophic Flagellates. Clarendon Press, Oxford. p. 113–131.

Christen, H. R. 1958. *Gymnodinium nygaardi* sp. nov. *Ber. Schweiz. Bot. Ges.*, 68:44–49.

Craveiro, S. C., Calado, A. J., Daugbjerg, N. & Moestrup, Ø. 2009. Ultrastructure and LSU rDNA-based revision of *Peridinium* group palatinum (Dinophyceae) with the description of *Palatinus* gen. nov. *J. Phycol.*, 45:1175–1194.

Craveiro, S. C., Daugbjerg, N., Moestrup, Ø. & Calado, A. J. 2015. Fine-structural characterization and phylogeny of *Peridinium polonicum*, type species of the recently described genus *Naiadinium* (Dinophyceae). *Eur. J. Protistol.*, 51:259–279.

Craveiro, S. C., Moestrup, Ø., Daugbjerg, N. & Calado, A. J. 2010. Ultrastructure and large subunit rDNA-based phylogeny of *Sphaerodinium cracoviense*, an unusual freshwater dinoflagellate with a novel type of eyespot. *J. Eukaryot. Microbiol.*, 57:568–585.

Craveiro, S. C., Pandeirada, M. S., Daugbjerg, N., Moestrup, Ø. & Calado, A. J. 2013. Ultrastructure and phylogeny of *Theleodinium calcisporum* gen. et sp. nov., a freshwater dinoflagellate that produces calcareous cysts. *Phycologia*, 52:488–507.

Darriba, D., Taboada, G. L., Doallo, R. & Posada, D. 2012. jModelTest 2: more models, new heuristics and parallel computing. *Nat. Methods*, 9:772.

Daugbjerg, N., Andreasen, T., Happel, E., Pandeirada, M. S., Hansen, G., Craveiro, S. C., Calado, A. J. & Moestrup, Ø. 2014. Studies on woloszynskioid dinoflagellates VII: description of *Borghiella andersenii* sp. nov.: light and electron microscopy and phylogeny based on LSU rDNA. *Eur. J. Phycol.*, 49:436–449.

Daugbjerg, N., Hansen, G., Larsen, J. & Moestrup, Ø. 2000. Phylogeny of some of the major genera of dinoflagellates based on ultrastructure and partial LSU rDNA sequence data, including the erection of three new genera of unarmoured dinoflagellates. *Phycologia*, 39:302–317.

Fábregas, J., Domínguez, A., Álvarez, D. G., Lamela, T. & Otero, A. 1998. Induction of astaxanthin accumulation by nitrogen and magnesium deficiencies in *Haematococcus pluvialis*. *Biotechnol. Lett.*, 20:623–626.

Frassanito, R., Cantonati, M., Tardìo, M., Mancini, I. & Guella, G. 2005. On-line identification of secondary metabolites in freshwater microalgae and cyanobacteria by combined liquid chromatography-photodiode array detection-mass spectrometric techniques. *J. Chromatogr. A*, 1082:33–42.

Frassanito, R., Flaim, G., Mancini, I. & Guella, G. 2006. High production of unexpected carotenoids in Dinophyceae. Astaxanthin esters from the freshwater dinoflagellate *Tovellia sanguinea*. *Biochem. Syst. Ecol.*, 34:843–853.

Guindon, S. & Gascuel, O. 2003. A simple, fast, and accurate algorithm to estimate large phylogenies by maximum likelihood. *Syst. Biol.*, 52:694–704.

Han, D., Li, Y. & Hu, Q. 2013. Astaxanthin in microalgae: pathways, functions and biotechnological implications. *Algae*, 28:131–147.

Hansen, G. & Moestrup, Ø. 1998. Fine-structural characterization of *Alexandrium catenella* (Dinophyceae) with special emphasis on the flagellar apparatus. *Eur. J. Phycol.*, 33:281–291.

Jeong, H. J., Jang, S. H., Moestrup, Ø., Kang, N. S., Lee, S. Y., Potvin, É. & Noh, J. H. 2014. *Ansanella granifera* gen. et sp. nov. (Dinophyceae), a new dinoflagellate from the coastal waters of Korea. *Algae*, 29:75–99.

Lenaers, G., Maroteaux, L., Michot, B. & Herzog, M. 1989. Dinoflagellates in evolution. A molecular phylogenetic analysis of large subunit ribosomal RNA. *J. Mol. Evol.*, 29:40–51.

Li, Z., Shin, H. H. & Han, M. 2015. Morphology and phylogeny of a new woloszynskioid dinoflagellate *Tovellia paldangensis* sp. nov. (Dinophyceae). *Phycologia*, 54:67–77.

Lindberg, K., Moestrup, Ø. & Daugbjerg, N. 2005. Studies on woloszynskioid dinoflagellates I: *Woloszynskia coronata* re-examined using light and electron microscopy and partial LSU rDNA sequences, with description of *Tovellia* gen. nov. and *Jadwigia* gen. nov. (Tovelliaceae fam. nov.). *Phycologia*, 44:416–440.

Lindström, K. 1991. Nutrient requirements of the dinoflagellate *Peridinium gatunense*. *J. Phycol.*, 27:207–219.

Luo, Z., You, X., Mertens, K. N. & Gu, H. 2016. Morphological and molecular characterization of *Tovellia* cf. *aveirensis* (Dinophyceae) from Jiulong River, China. *Nova Hedwigia*, 103:79–94.

Moestrup, Ø. & Calado, A. J. 2018. Dinophyceae. *In:* Büdel, B., Gärtner, G., Krienitz, L. & Schagerl, M. (ed.), Süsswasserflora von Mitteleuropa — Freshwater Flora of Central Europe, vol. 6, 2nd ed., Springer-Verlag, Berlin. XII + 561 pp.

Moestrup, Ø. & Daugbjerg, N. 2007. On dinoflagellate phylogeny and classification. *In:* Brodie, J. & Lewis, J. (ed.), Unravelling the Algae. The Past, Present, and Future of Algal Systematics. CRC Press, Boca Raton, FL. Systematics Association Special Volume No. 75:215–230.

Moestrup, Ø., Hansen, G., Daugbjerg, N., Flaim, G. & D'Andrea, M. 2006. Studies on woloszynskioid dinoflagellates II: on *Tovellia sanguinea* sp. nov., the dinoflagellate responsible for the reddening of Lake Tovel, N. Italy. *Eur. J. Phycol.*, 41:47–65.

Mulders, K. J. M., Weesepoel, Y., Bodenes, P., Lamers, P. P., Vincken, J., Martens, D. E., Gruppen, H. & Wijffels, R. H. 2015. Nitrogen-depleted *Chlorella zofingiensis* produces astaxanthin, ketolutein and their fatty acid esters: a carotenoid metabolism study. *J. Appl. Phycol.*, 27:125–140.

Orosa, M., Valero, J. F., Herrero, C. & Abalde, J. 2001. Comparison of the accumulation of astaxanthin in *Haematococcus pluvialis* and other green microalgae under N-starvation and high light conditions. *Biotechnol. Lett.*, 23:1079–1085.

Pandeirada, M. S., Craveiro, S. C. & Calado, A. J. 2013. Freshwater dinoflagellates in Portugal (W Iberia): a critical checklist and new observations. *Nova Hedwigia*, 97:321–348.

Pandeirada, M. S., Craveiro, S. C., Daugbjerg, N., Moestrup, Ø. & Calado, A. J. 2014. Studies on woloszynskioid dinoflagellates VI: description of *Tovellia aveirensis* sp. nov. (Dinophyceae), a new species of Tovelliaceae with spiny cysts. *Eur. J. Phycol.*, 49:230–243.

Pandeirada, M. S., Craveiro, S. C., Daugbjerg, N., Moestrup, Ø. & Calado, A. J. 2017. Studies on woloszynskioid dinoflagellates VIII: life cycle, resting cyst morphology and phylogeny of *Tovellia rinoi* sp. nov. (Dinophyceae). *Phycologia*, 56:533–548.

Popovský, J. & Pfiester, L. A. 1990. Dinophyceae (Dinoflagellida). *In:* Ettl, H., Gerloff, J., Heynig, H. & Mollenhauer, D. (ed.), Süsswasserflora von Mitteleuropa, Vol. 6. G. Fischer, Jena. p. 272.

Remias, D., Pichrtová, M., Pangratz, M., Lütz, C. & Holzinger, A. 2016. Ecophysiology, secondary pigments and ultrastructure of *Chlainomonas* sp. (Chlorophyta) from the European Alps compared with *Chlamydomonas nivalis* forming red snow. *FEMS Microbiol. Ecol.*, 92:1–11.

Roberts, K. R. 1989. Comparative analyses of the dinoflagellate flagellar apparatus. II. *Ceratium hirundinella*. *J. Phycol.*, 25:270–280.

Roberts, K. R., Hansen, G. & Taylor, F. J. R. 1995. General ultrastructure and flagellar apparatus architecture of *Woloszynskia limnetica* (Dinophyceae). *J. Phycol.*, 31:948–957.

Roberts, K. R. & Timpano, P. 1989. Comparative analyses of the dinoflagellate flagellar apparatus. I. *Woloszynskia* sp. *J. Phycol.*, 25:26–36.

Ronquist, F. & Huelsenbeck, J. P. 2003. MrBayes 3: Bayesian phylogenetic inference under mixed models. *Bioinformatics*, 19:1572–1574.

Salgado, P., Fraga, S., Rodríguez, F. & Bravo, I. 2018. Benthic flattened cells of the phylogenetically related marine dinoflagellates *Protoceratium reticulatum* and *Ceratocorys mariaovidiorum* (Gonyaulacales): a new type of cyst? *J. Phycol.*, 54:138–149.

Santos, M. F. & Mesquita, J. F. 1984. Ultrastructural study of *Haematococcus lacustris* (Girod.) Rostafinksi (Volvocales) I. Some aspects of carotenogenesis. *Cytologia*, 49:215–228.

Sarma, Y. S. R. K. & Shyam, R. 1974. On the morphology, reproduction and cytology of two freshwater dinoflagellates from India. *Brit. Phycol. J.*, 9:21–29.

Scholin, C. A., Herzog, M., Sogin, M. & Anderson, D. M. 1994. Identification of group- and strain-specific genetic markers for globally distributed *Alexandrium* (Dinophyceae). II. Sequence analysis of a fragment of the LSU rRNA gene. *J. Phycol.*, 30:999–1011.

Shyam, R. & Sarma, Y. S. R. K. 1976 ('1975'). *Woloszynskia stoschii* and *Gymnodinium indicum*, two new freshwater dinoflagellates from India: morphology, reproduction and cytology. *Plant Syst. Evol.*, 124:205–212.

Solovchenko, A. E. 2015. Recent breakthroughs in the biology of astaxanthin accumulation by microalgal cell. *Photosynth. Res.*, 125:437–449.

Stosch, H. A. 1973. Observations on vegetative reproduction and sexual life cycles of two freshwater dinoflagellates. *Gymnodinium pseudopalustre* Schiller and *Woloszynskia apiculata* sp. nov. *Brit. Phycol. J.*, 8:105–134.

Swofford, D. L. 2003. PAUP*: phylogenetic analysis using parsimony (*and other Methods), Version 4. Sinauer Associates, Sunderland, MA.

Takano, Y. & Horiguchi, T. 2005. Acquiring scanning electron microscopical, light microscopical and multiple gene sequence data from a single dinoflagellate cell. *J. Phycol.*, 42:251–256.

Thompson, R. H. 1951 ('1950'). A new genus and new records of freshwater Pyrrophyta in the Desmokontae and Dinophyceae. *Lloydia*, 13:277–299.

Turland, N. J., Wiersema, J. H., Barrie, F. R., Greuter, W., Hawksworth, D. L., Herendeen, P. S., Knapp, S., Kusber, W.-H., Li, D.-Z., Marhold, K., May, T. W., McNeill, J., Monro, A. M., Prado, J., Price, M. J. & Smith, G. F. (ed.) 2018. International Code of Nomenclature for algae, fungi, and plants (Shenzhen Code) adopted by the Nineteenth International Botanical Congress Shenzhen, China, July 2017. Koeltz Botanical Books, Glashütten. XXXVIII + 254 pp. (Regnum Vegetabile vol. 159). https://doi.org/10.12705/code.2018

Wołoszyńska, J. 1917. Nowe gatunki Peridineów, tudzież spostrzeżenia nad budową okrywy u Gymnodiniów i Glenodiniów. — Neue Peridineen-Arten, nebst Bemerkungen über den Bau der Hülle bei *Gymno-* und *Glenodinium*. *Bull. Int. Acad. Sci. Cracovie, Cl. Sci. Math., Sér. B, Sci. Nat.*, 1917:114–122, pls 11–13.

Zhang, Q., Zhu, H., Hu, Z. & Liu, G. 2016. Blooms of the woloszynskioid dinoflagellate *Tovellia diexiensis* sp. nov. (Dinophyceae) in Baishihai Lake at the eastern edge of Tibetan Plateau. *Algae*, 31:205–217.